Iranian Journal of Medical Physics

ijmp.mums.ac.ir

Dynamic ^{18}F-FDG PET Images Simulation Using 4D-XCAT Phantom and Kinetic Modeling for Lesion Detectability Investigation and Scan Time Reduction Purpose

Fethi Bezoubiri[1*], Tahar Zidi[2], Fayçal Kharfi[3,4]

1. Radiological and Atomic Physics Department, Physics Division, Nuclear Research Center of Algiers, 16000, Algiers, Algeria.
2. Atomic Energy Commission (COMENA), Algiers, Algeria.
3. Department of Physics, Faculty of Sciences, Ferhat Abbas-Setif1 University, Campus El-Bèz, Sétif-19000, Algeria.
4. Laboratory of Dosing, Analysis and Characterization with High Resolution (DAC), Ferhat Abbas-Setif1University, Campus El-Bèz, Sétif-19000, Algeria

ARTICLE INFO

Article type:
Original Paper

Article history:
Received: Nov 28, 2022
Accepted: May 13, 2023

Keywords:
Computer Simulation
Positron-Emission Tomography
Imaging Phantom
Image Reconstruction

ABSTRACT

Introduction: Simulation in Positron Emission Tomography (PET) studies is considered as an effective approach to test new mathematical methods for image processing and lesion detection. It's an alternative way to overcome the drawback of obtaining a sufficient set of clinical images with known truth about the presence or absence of lesions. This work aimed to simulate, in a new and fast way, realistic dynamic ^{18}F-FDG PET images for lesion detectability investigation and scan time reduction.

Material and Methods: The 4D-XCAT phantom was utilized in this work. The three-compartment model was used to simulate the Time Activity Curves (TAC's) of ^{18}F-FDG. The arterial input function of ^{18}F-FDG was modeled using a parametric function. The TAC's of 11 tissues defined in the 4D-XCAT phantom were simulated. The activity values were calculated from the TAC's considering a real ^{18}F-FDG dynamic PET acquisition protocol. These activity values were assigned to each voxel of 4D-XCAT to produce 28 activity maps. The GE Discovery PET/CT 710 scanner, modeled in the STIR platform, was used to generate the sinograms. OSMAPOSL Algorithm was considered to reconstruct dynamic ^{18}F-FDG PET images.

Results: Realistic dynamic ^{18}F-FDG PET images were generated. The qualitative and quantitative comparison showed a good agreement between the 4D-XCAT phantom images before and after the reconstruction procedure. The computation time of the reconstruction procedure was 8.76 min/frame.

Conclusion: The present study was found to be a promising and realistic approach to dynamic PET dPET imaging optimization in terms of scanning time reduction and lesion detectability amelioration.

► *Please cite this article as:*
Bezoubiri F, Zidi T, Kharfi F. Dynamic ^{18}F-FDG PET Images Simulation Using 4D-XCAT Phantom and Kinetic Modeling for Lesion Detectability Investigation and Scan Time Reduction Purpose. Iran J Med Phys 2024; 21: 84-92. 10.22038/IJMP.2023.69200.2216.

Introduction

Positron emission tomography (PET) is a medical imaging modality widely used in nuclear medicine for cancer diagnosis. It allows three-dimensional distribution measurements of a molecule marked by a positron emitter. Dynamic PET acquisition with [18F] FluoroDeoxyGlucose (dPET 18F-FDG) plays an important role in the initial diagnosis and characterization of tumour [1-4]. It is often used with kinetic modeling to estimate the physiological parameters that characterize the functional state of tissue, such as 18F-FDG metabolic rate. However, dPET remains limited to research since it suffers from several drawbacks such as long-time duration of data acquisition and the high noise of the images [5, 6].

Several works have been performed on dPET to improve tumor detection and reduce the scanning time using patient data [7-10]. In the work of Fahrni et al [10], it has been shown that the parametric images issued from dPET can improve tumor detectability. Grkovski et al., [7] have shown that the acquisition time could be reduced to 20 min in the case of head and neck cancers. The kinetic parameters obtained were rather equivalent in a comparison study investigated by Torizuka et al [8] using 30 min and 60 min acquisition protocols. The work of Visser et al. [9] on 13 patients with non-small cell lung carcinoma found an agreement between 30 min and 50 min acquisition protocols. However, the most drawback of using the clinical images is to obtain a sufficient set of clinical images with known truth about the presence or absence of lesions. Furthermore, the patient clinical data aren't always available. To overcome these drawbacks, the simulation approach is highly recommended. It is considered a substantial way for researchers to provide images for developing and testing new mathematical methods for image

*Corresponding Author: Tel: +213 21 43 44 44 poste 1320; Email: f.bezoubiri@crna.dz ; fethino@yahoo.fr

processing and lesion detection. The simulated images can be considered clinically realistic if a validated PET imaging system combined with a realistic model of the human body and an actual 18F-FDG activity distribution are used [11].

Many studies have been carried out to simulate the dynamic 18F-FDG PET images with different approaches and purposes. Karakatsanis et al. [12], simulated dynamic 18F-FDG PET images using 4D-XCAT phantom and the Monte Carlo (MC) code GATE to optimize clinical whole-body parametric imaging protocols. However, the MC simulation is time-consuming. Häggström et al. [13], developed Dynamic PET Step, dPETSTEP, a simulator for dPET simulations in order to study the kinetic modeling and parametric images. This simulator is based on simple scatter and random models, which make it as not appropriate to study these phenomena.

Karakatsanis et al. [14] utilized a numerical phantom combined with the Software for Tomographic Image Reconstruction (STIR) to generate simulated images with different levels of Poisson noise. STIR is a powerful tool for image reconstruction and simulation. It offers a range of reconstruction algorithms, including filtered back projection, expectation-maximization, and Ordered Subsets Expectation-Maximization (OSEM). However, users may need to handle a considerable number of functions to perform simulations effectively.

Hence, this work aimed to simulate, in an easy and fast way, realistic dynamic ^{18}F-FDG PET images for lesion detectability investigation and scan time reduction purposes. To do so, the well-known 4D Extended Cardiac-Torso (4D-XCAT) phantom and the Software for Tomographic Image Reconstruction (STIR) were used. Time Activity Curves (TAC's) of the different tissues of the 4D-XCAT phantom were calculated using the three-compartment model and simulated input function. To efficiently perform the simulation, an in-house MATLAB program was implemented to connect the simulation parts and to handle all STIR functions used in this work.

Materials and Methods

Activity maps based on numerical phantom

In this study, we have used the realistic 4D-XCAT human torso phantom to model the time-dependent activity and the 511 keV attenuation maps [15, 16]. This phantom has found numerous applications in different domains such as radiotherapy and imaging [15, 16, 17, 18, 19, 20].

The phantom used in our work contained 1200 slices with a voxel size of 2.5 x 2.5 x 2.5 mm^3. The image matrix size was 256 × 256 pixels. A lesion of 9 mm diameter was modeled and inserted at the top of the liver in the main phantom 4D-XCAT. The attenuation maps generated were used for the attenuation correction in the image reconstruction procedure.

The activity maps were generated following four steps:

Step 1 includes the calculation of TAC's for different tissues of the 4D-XCAT phantom. The calculation was performed using actual ^{18}F-FDG kinetic micro-parameters, an effective blood plasma volume values (see Table 1) [21-22], and a modeled input function. In step 2, a series of dynamic activity maps were generated using a real acquisition protocol. The protocol used consists of 28 frames recorded during 55 min: 9*10s, 3*30s, 4*60s, 4*120s and 8*300s [23]. Step 3 concerns the calculation of the activity values according to each time frame. In step 4, the calculated activity values were assigned to the voxels of each region of the 4D-XCAT phantom to produce 28 activity maps. The whole steps followed to generate the activity maps are illustrated in figure 1. These steps were performed using in-house script implemented in MATLAB environment, version R2017a.

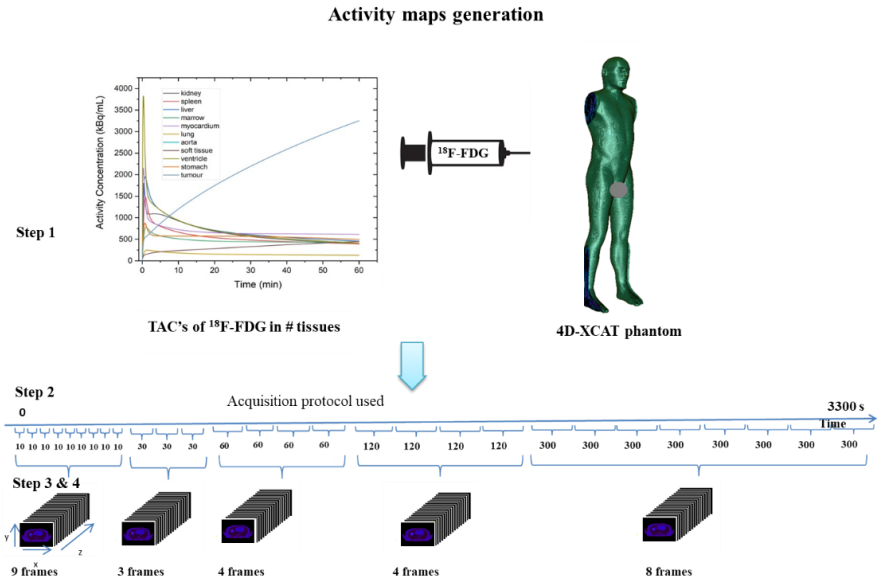

Figure 1. Steps followed to generate the activity maps

Modelization of the ^{18}F-FDG Time Activity Curves

The TAC's of ^{18}F-FDG were generated using the standard three-compartment model [24]. A descriptive schema of this model is illustrated in figure 2.

In the model used, $C_p(t)$ is the input function, $C_e(t)$ and $C_m(t)$ are the concentrations of unmetabolized, metabolized and trapped ^{18}F-FDG in tumor cells, respectively, expressed in kBq/mL.

- $k_{1\to4}$ are parameters describing the exchanges between the compartments.
- k_1 (min^{-1}) and k_2 (min^{-1}) represent the reversible exchanges of FGD between the blood and tissue compartments;
- k_3 (min^{-1}) represents the phosphorylation of the FDG ^{18}FDG-6-P_{O4};
- k_4 (min^{-1}) represents the effect of possible dephosphorylation of FDG-6-PO_4 to ^{18}F-FDG.

The values of these parameters, as reported in the literature, are given in the Table 1.

The ^{18}F-FDG kinetics is described by the following differential equations:

$$\frac{dC_e(t)}{dt} = k_1 C_p(t) - (k_2 + k_3) C_e(t) + k_4 C_m(t) \quad (1)$$

$$\frac{dC_m(t)}{dt} = k_3 C_e(t) - k_4 C_m(t) \quad (2)$$

$$C_{FDG}(t) = C_e(t) + C_m(t) + V_p C_p(t) \quad (3)$$

$C_{FDG}(t)$ being the total concentration of the ^{18}F-FDG in a Region Of Interest (ROI), and V_p represents the effective blood plasma volume contained in the ROI.

The solution of this system of equation gives:

$$C_{FDG} = K_i \int C_p(t)dt + V_p C_p(t) \quad (4)$$

With: $$K_i = \frac{k_1 * k_3}{k_2 + k_3} \quad (5)$$

To generate the ^{18}F-FDG TAC's, we have modeled the input function $C_p(t)$ using the parametric function proposed by D. Feng [25-28]. The mathematical expression of this model is given as follows:

$$C_p(t) = (A_1 t - A_2 - A_3)e^{\lambda_1 t} + A_2 e^{\lambda_2 t} + A_3 e^{\lambda_3 t} \quad (6)$$

with:

- λ_1 (min^{-1}), λ_2 (min^{-1}) and λ_3 (min^{-1}) are the eigenvalues of the model.
- A_1 (μCi/ml/min), A_2 (μCi/ml) and A_3(μCi/ml) are the coefficients of the model.

The values of the $\lambda_{1\to3}$ and $A_{1\to3}$ are repoted in table 2.

Table 1. The ^{18}F-FDG kinetic micro-parameters and effective blood plasma volume V_p used for the different organs.

organs	k_1 (ml/min/ml)	k_2 (min^{-1})	k_3 (min^{-1})	k_4 (min^{-1})	V_p
kidney	0.2630	0.2990	0.0000	0.0000	0.4380
spleen	1.2070	1.9090	0.0080	0.0140	0.0000
liver	1.2560	1.3290	0.0020	0.0020	0.1650
marrow	0.4250	1.0550	0.0230	0.0130	0.0400
myocardium	0.1960	1.0220	0.1490	0.0100	0.5450
lung	0.1080	0.7350	0.0160	0.0130	0.0170
aorta	0.0000	0.0000	0.0000	0.0000	1.0000
soft tissue	0.0470	0.3250	0.0840	0.0000	0.0190
ventricle	0.0000	0.0000	0.0000	0.0000	1.0000
stomach	0.6140	1.8850	0.0710	0.0310	0.0630
tumour	0.1860	0.4380	0.3360	0.0000	0.0800

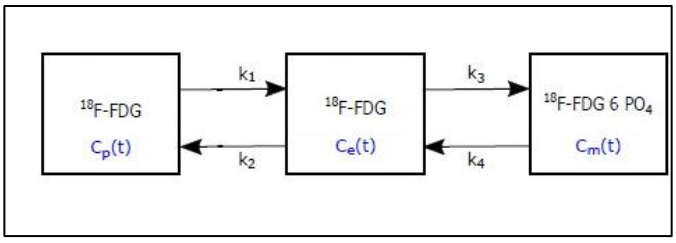

Figure 2. A schema showing the three-compartment model of 18F-FDG uptake. $k_{1\to4}$ are the parameters describing the exchanges between the compartments. $C_p(t)$ is the input function. $C_e(t)$ and $C_m(t)$ are the concentrations of unmetabolized, metabolized and trapped 18F-FDG in tumor cells, respectively.

Table 2. Coefficients and eigenvalues of the parametric function used to model the input function.

A_1 (μCi/ml/min)	A_2 (μCi/ml)	A_3 (μCi/ml)	λ_1 (min^{-1})	$\boldsymbol{\lambda_2}$ (min^{-1})	$\boldsymbol{\lambda_3}$ (min^{-1})
851.1225	21.8798	20.8113	-4.1339	-0.1191	-0.0104

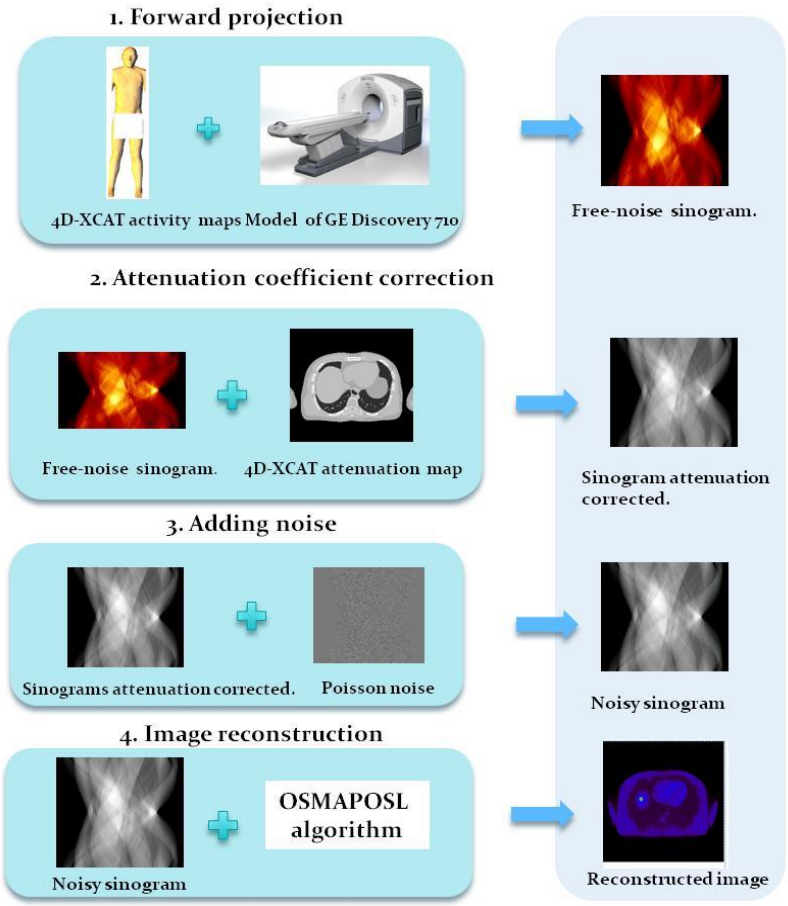

Figure 3. Workflow showed the steps followed in the reconstruction procedure.

Scanner geometry, sinograms generation and image reconstruction

In this study, STIR software version 4.0.0-alpha was employed [29]. Firstly, we have used STIR ray tracing technique to perform the forward projection of the 4D-XCAT activity maps in order to generate a free-noise sinograms. The model of Discovery PET/CT 710 scanner manufactured by General Electric (GE) Healthcare Company was considered. The main physical characteristics of this scanned are reported in Table 3. Secondly, the free-noise sinograms generated were attenuation corrected by calculating the attenuation coefficient from the 4D-XCAT attenuation maps. Then, a noisy sinograms were obtained by corrupting the corrected sinograms with Poisson noise. Finally, these sinograms were reconstructed using Ordered Subsets-Maximum A posteriori Probability-One Step Late (OSMAPOSL) algorithm with 35 iterations and 1 subset**.** The same reconstruction procedure was applied to all the 28 frames covering the liver region. The reconstructed image size was 256 x 256 pixels, with the voxel size of 2.5 x 2.5 mm^2. The steps of the reconstruction procedure were shown in Figure 3.

We have implemented and used a MATLAB script to handle and connect all STIR functions used, from the forward projection to the reconstruction. The script was run on workstation HP Z8 64 using PARFOR (PARallel FOR) loop. This loop was used to execute iterations in parallel, which can significantly improve the performance of computations on multi-core processors. It's similar to the standard FOR loop but with the added capability of parallel execution. The workstation used, powered with Windows 10, is equipped with 20 physical CPUs, Intel© Xeon© Silver 4210 CPU @2.20 GHz, 64 GB RAM, and NVIDIA Quadro P400 graphic card with 2 GB RAM.

The qualitative and quantitative evaluation of the images reconstructed were performed using AMIDE open source software, version 1.0.4 [30].

Results

The input function obtained using equation 6 and the parameters values reported in Table 2, is given in Figure 4-A. TAC of 11 tissues modeled in 4D-XCAT phantom were generated, assuming the standard 3-compartment model, the calculated input function and kinetic physiological parameters of the ^{18}F-FDG. The TAC's generated are illustrated in Figure 4-B. As it is well shown in Figure 4-A & 4-B, the metabolic characteristics of the ^{18}F-FDG in terms of injection, uptake, and elimination are distinctive.

The TAC's obtained were used to generate the ^{18}F-FDG dynamic activity maps.

Figure 5 shows the transverse, coronal and sagittal slices of the ^{18}F-FDG activity maps. These slices were selected from the 1st, 17th and 28th frames among the 28 frames generated to show the effect of the reconstruction procedure when the activity concentration in the lesion is lower, equal and higher than the background (liver).

The whole generated frames were forward projected and reconstructed using in-house script connecting STIR functions needed. The projection data of frame 28 is shown in Figure 6. The reconstructed images of those shown in Figure 5 are displayed in Figure 7. Each frame contained 47 slices. The quantitative analysis of the images reconstructed was performed via the calculation of the line profiles traced on a transverse slice of the images illustrated in Figure 5 & 7. Figure 8 illustrates the line profiles obtained.

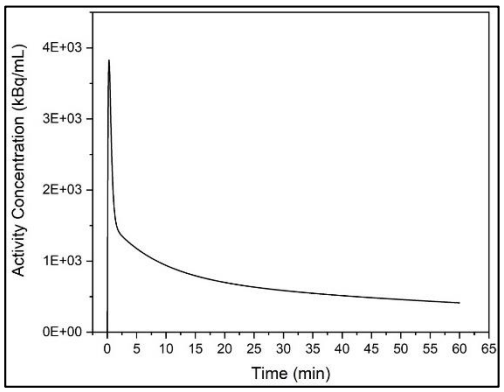

Figure 4-A. 18F-FDG Input function used in this study

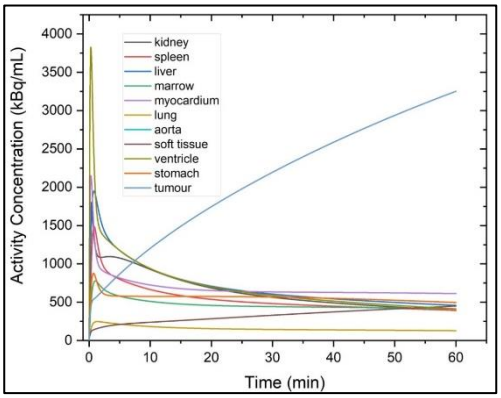

Figure 4-B. TAC's of ^{18}F-FDG generated in different tissues

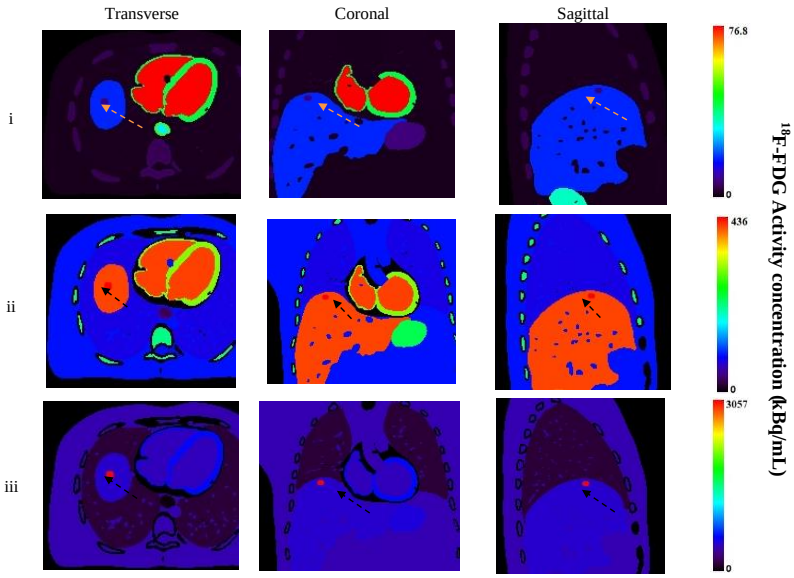

Figure 5. Transverse, coronal and sagittal images of ^{18}F-FDG activity maps taken at 3 different time points corresponding to : i = frame 1, ii = frame 17 and iii = frame 28. The arrow shows the lesion inserted in the liver

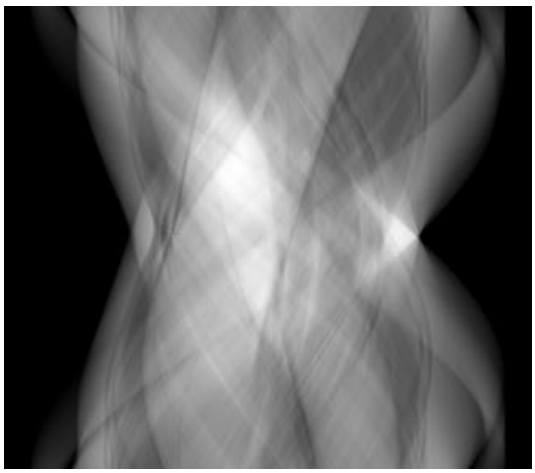

Figure 6. A sinogram of the activity maps of frame 28 obtained during forward projection step using Discovery PET/CT 710 scanner model.

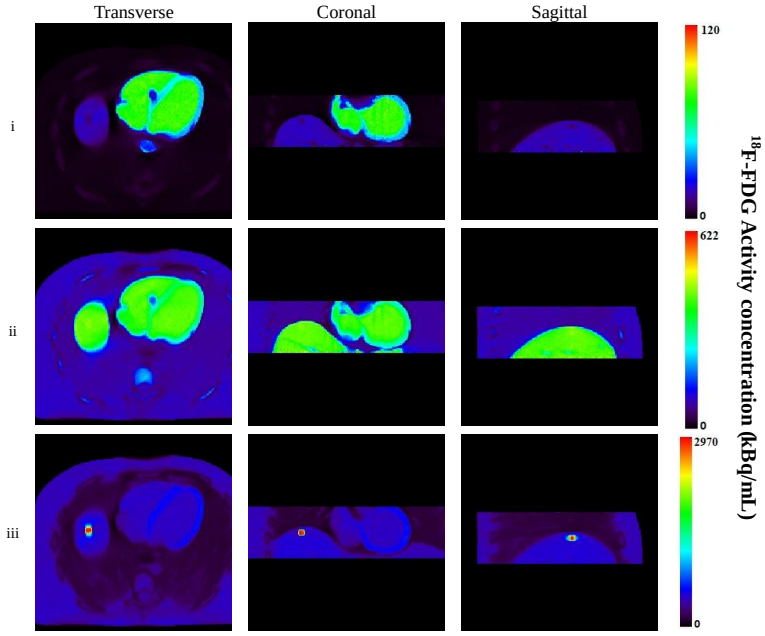

Figure 7. Transverse ,coronal and sagittal reconstructed 18F-FDG PET images taken at 3 different time points corresponding to i = frame 1, ii = frame 17 and iii = frame 28.

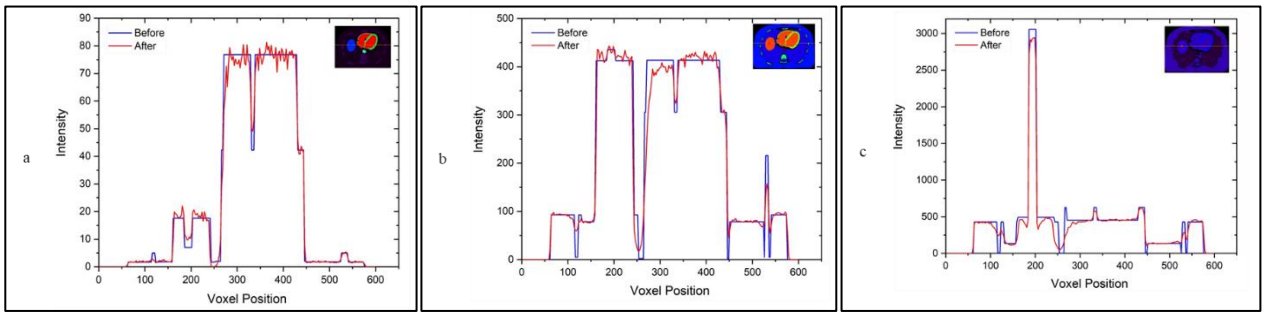

Figure 8. Line profiles through a transverse slice of 4D-XCAT phantom before and after reconstruction: (a) frame 1, (b) frame 17, (c) frame 28

Discussion

dPET remains limited to research since it suffers from several drawbacks such as high noise of the images and the long-time duration of data acquisition. Several attempts have been made to overcome these drawbacks using patient data. However, the unavailability of clinical data and the absence of gold standard slow down the development of this technique

for clinical uses. To overcome these limitations, we have proposed a new methodology to simulate realistic dynamic ^{18}F-FDG PET images using realistic model of human body, 4D-XCAT phantom, combined with the three-compartment model, an actual acquisition protocol and simulated input function. ^{18}F-FDG PET images obtained were reconstructed using STIR software. We have used in-house script developed to generate different tissues TAC's, manipulate 4D-XCAT phantom and handle all STIR functionalities such as data forward protection, attenuation correction, noise adding to the sinograms and images reconstruction. The computation time was 8.76 min/frame.

In Figure 4-B, the simulated TAC's curves of the phantom tissues clearly show the tracer uptake and clearance, while the TAC of the tumor reveals a continuous tracer trapping. This behavior is correlated with the constant values k_3 and k_4 as it can be deduced from table 1. The TAC's derived for the ventricles and the aorta are similar and evidently, reproduce the behavior of the input function since all the kinetic micro-parameters of these organs are equal to zero and the effective blood plasma volume is equal to one.

In Figure 5, as expected, the activity is highest in the ventricles and the aorta as it can be seen in the images of frame 1. The lesion appears as a cold spot because at this step, the tumor has lower activity than the surrounding tissue. In the case of the image selected from frame 17, the lesion could not be recognized as the activity values in the tumor and in the liver are almost the same. The tumor can however, be accurately detected in the case of frame 28 where the ^{18}F-FDG trapping is high and irreversible.

From Figure 5 and Figure 7, the qualitative comparison shows that the images before and after the reconstruction were very similar. However, the lesion not clearly apparent in the frame 17 since the lesion and liver activity values were close, can be not seen in the corresponding reconstructed image. This is due to the technical limitations of the scanner model used in this study.

In Figure 8, we can observe that the voxel intensities of the transverse images before and after reconstruction procedure are almost the same. The qualitative and quantitative comparison has demonstrated the efficiency of the reconstruction procedure followed in the present study.

It is worth mentioning that dynamic ^{18}F-FDG PET images simulation using 4D-XCAT phantom with kinetic modeling, and real patient clinical data differ in several ways. First of all, images from 4D-XCAT phantom and kinetic modeling simulations aim to replicate realistic human anatomy and physiology, but they are still computer-generated and may not fully capture the complexity of real patient data. Real patient data is obtained from actual patient scans and thus reflects the variability and diversity of real-world patients. Secondly, simulation methods can control the level and type of noise and artifacts present in the images, whereas real patient data may contain various types of noise and artifacts due to patient motion, scanner hardware, or other factors. The patient-specific characteristics such as age, body size, and co-morbidities can significantly affect the results of PET imaging. Simulation methods may not fully replicate these characteristics and the associated variability that is present in real patient data. Finally, the experimental conditions for 4D-XCAT phantom and kinetic modeling simulation are controlled and standardized, whereas real patient data may vary in terms of the radiotracer dose, uptake time, and imaging parameters used.

Despite these differences, 4D-XCAT phantom and kinetic modeling simulations can be useful for understanding the underlying physics and limitations of PET imaging and for developing and testing imaging algorithms and techniques. Real patient data, on the other hand, is essential for clinical decision-making and patient care, and provides a more comprehensive understanding of the disease process and the effects of treatment.

Many studies were recently undertaken on the interest of dynamic ^{18}F-FDG PET simulation and kinetic modeling such as that of Dimitrakopoulou-Strauss et al. [5]. This last study focused on the use of kinetic modeling and parametric imaging with dynamic PET for oncological applications, which is a broader topic than just lesion detectability investigation. Our work reinforces and supports the main findings of Dimitrakopoulou-Strauss et al. study and resolve some mentioned problems such as the problem of time-consuming. Indeed, Dimitrakopoulou-Strauss et al. reported that kinetic modeling and parametric imaging can be used to improve lesion detectability in oncological PET imaging. Similarly, both the 4D-XCAT phantom and kinetic modeling approaches have been shown to be effective in detecting lesions in dynamic ^{18}F-FDG PET images. In terms of quantitative accuracy, Dimitrakopoulou-Strauss et al. emphasized the importance of quantitative accuracy in oncological PET imaging. The study by Dimitrakopoulou-Strauss et al. also discussed the computational complexity of kinetic modeling, which can be time-consuming and require significant computing resources. Similarly, the 4D-XCAT phantom approach can be computationally intensive.

The comparison between research works as our actual one on dynamic ^{18}F-FDG PET images simulation using 4D-XCAT phantom and kinetic modeling for lesion detectability investigation is more focused on a specific application of some simulation and kinetics methods. However, all undertaken studies highlight the importance of quantitative accuracy and the computational complexity of these approaches. Indeed, different used methods have been shown to be effective in detecting lesions, with some studies reporting similar lesion detectability. However, there have been some reports of differences in lesion detectability depending on factors such as lesion size and location.

The data generated through this work can be used to study the reduction of the total duration of data

acquisition in dPET while preserving the detectability of lesions by applying the multivariate image analysis techniques such as Principal Component Analysis (PCA). This could be investigated by extracting relevant images from the simulated dynamic imaging sequences that provide a lesion detectability level similar to the usual static images acquired at 35 mins post-injection. Full length and shorter dynamic sequences can be analyzed both qualitatively and quantitatively to demonstrate the potential of the proposed methodology. Other methods to reduce the total duration of dynamic PET imaging with ^{18}F-FDG include sparse sampling schemes, multi-parametric image reconstruction, and deep learning-based techniques. However, these methods are still in the early stages of development and require further validation before they can be routinely used in clinical practice.

Even though we have considered in this work only one lesion in the liver, the study could be easily extended to insert lesions with different shapes and concentrations in various organs. The effect of the respiratory motion on the reconstructed images will also be considered.

Conclusion

In this study, simulation of dynamic ^{18}F-FDG PET images using 4D-XCAT phantom and kinetic modeling has shown promise in lesion detectability investigation and scan time reduction purposes. Lesion detectability investigation studies have shown that using 4D-XCAT phantom with kinetic modeling approach can be effective in detecting lesions in dynamic ^{18}F-FDG PET images. Kinetic modeling with 4D-XCAT phantom simulations is found to be more accurate in estimating kinetic parameters and for lesion localization, things that are very important for quantitative analysis and treatment planning. The methodology proposed in this work is based on the combination between a 3-compartment model, 4D-XCAT Digital Phantom, and STIR software. Thus, an in-house program was implemented in parallel pool on MATLAB environment to connect and handle all parts of the performed simulations and to facilitate the use of STIR functions.

Regarding the scan time reduction, 4D-XCAT phantom with kinetic modeling simulation can be useful in identifying the optimal scan time and duration that can achieve high lesion detectability with a reduced scan time. This is particularly important in clinical settings where scan time is a limiting factor, such as in pediatric or claustrophobic patients.

Overall, the use of 4D-XCAT phantom and kinetic modeling simulation in dynamic ^{18}F-FDG PET imaging can aid in lesion detectability investigation and scan time reduction, thus providing better patient care and improving the efficiency of clinical PET imaging. However, it is important to note that simulation results should always be validated against real patient data before being applied in clinical practice.

References

1. Besson FL, Fernandez B, Faure S, Mercier O, Seferian A, Mignard X, et al. 18 F-FDG PET and DCE kinetic modeling and their correlations in primary NSCLC: first voxel-wise correlative analysis of human simultaneous [18F] FDG PET-MRI data. EJNMMI research. 2020 Dec;10:1-3.
2. Zhuang M, Karakatsanis NA, Dierckx RA, Zaidi H. Impact of tissue classification in MRI-guided attenuation correction on whole-body Patlak PET/MRI. Molecular Imaging and Biology. 2019 Dec;21:1147-56.
3. Nozawa A, Rivandi AH, Kanematsu M, Hoshi H, Piccioni D, Kesari S, et al. Glucose-corrected standardized uptake value in the differentiation of high-grade glioma versus post-treatment changes. Nuclear medicine communications. 2015 Jun 1;36(6):573-81.
4. Rusten E, Rødal J, Bruland ØS, Malinen E. Biologic targets identified from dynamic 18FDG-PET and implications for image-guided therapy. Acta Oncologica. 2013 Oct 1;52(7):1378-83.
5. Dimitrakopoulou-Strauss A, Pan L, Sachpekidis C. Kinetic modeling and parametric imaging with dynamic PET for oncological applications: general considerations, current clinical applications, and future perspectives. European journal of nuclear medicine and molecular imaging. 2021 Jan;48:21-39.
6. Al-Enezi MS, Bentourkia MH. Kinetic Modeling of Dynamic PET-^{18}F-FDG Atherosclerosis Without Blood Sampling. IEEE Transactions on Radiation and Plasma Medical Sciences. 2020 Jun 30;4(6):729-34.
7. Grkovski M, Schöder H, Lee NY, Carlin SD, Beattie BJ, Riaz N, et al. Multiparametric imaging of tumor hypoxia and perfusion with 18F-fluoromisonidazole dynamic PET in head and neck cancer. Journal of Nuclear Medicine. 2017 Jul 1;58(7):1072-80.
8. Visser EP, Kienhorst LB, de Geus-Oei LF, Oyen WJ. Shortened dynamic FDG-PET protocol to determine the glucose metabolic rate in non-small cell lung carcinoma. In2008 IEEE Nuclear Science Symposium Conference Record. 2008:4455-8.
9. Torizuka T, Nobezawa S, Momiki S, Kasamatsu N, Kanno T, Yoshikawa E, et al. Short dynamic FDG-PET imaging protocol for patients with lung cancer. European journal of nuclear medicine. 2000 Oct;27:1538-42.
10. Fahrni G, Karakatsanis NA, Di Domenicantonio G, Garibotto V, Zaidi H. Does whole-body Patlak 18 F-FDG PET imaging improve lesion detectability in clinical oncology?. European radiology. 2019 Sep 1;29:4812-21.
11. Lee C. Monte carlo calculations in nuclear medicine second edition: Applications in diagnostic imaging. 2014; 431-2
12. Karakatsanis NA, Lodge MA, Tahari AK, Zhou Y, Wahl RL, Rahmim A. Dynamic whole-body PET parametric imaging: I. Concept, acquisition protocol optimization and clinical application: Physics in Medicine & Biology. 2013 Sep 30;58(20):7391.
13. Häggström I, Beattie BJ, Schmidtlein CR. Dynamic PET simulator via tomographic emission projection

for kinetic modeling and parametric image studies. Medical Physics. 2016 Jun;43(6Part1):3104-16.
14. Karakatsanis NA, Zhou Y, Lodge MA, Casey ME, Wahl RL, Zaidi H, et al. Generalized whole-body Patlak parametric imaging for enhanced quantification in clinical PET. Physics in Medicine & Biology. 2015 Oct 28;60(22):8643.
15. Segars WP, Sturgeon G, Mendonca S, Grimes J, Tsui BM. 4D XCAT phantom for multimodality imaging research. Medical physics. 2010 Sep;37(9):4902-15.
16. Segars WP, Tsui BM. MCAT to XCAT: The evolution of 4-D computerized phantoms for imaging research. Proceedings of the IEEE. 2009 Nov 17;97(12):1954-68.
17. Segars WP, Tsui BM, Cai J, Yin FF, Fung GS, Samei E. Application of the 4-D XCAT phantoms in biomedical imaging and beyond. IEEE transactions on medical imaging. 2017 Aug 10;37(3):680-92.
18. Nankali S, Torshabi AE, Miandoab PS, Baghizadeh A. Optimum location of external markers using feature selection algorithms for real-time tumor tracking in external-beam radiotherapy: a virtual phantom study. Journal of applied clinical medical physics. 2016 Jan;17(1):221-33.
19. Miandoab PS, Torshabi AE, Nankali S. Investigation of the optimum location of external markers for patient setup accuracy enhancement at external beam radiotherapy. Journal of applied clinical medical physics. 2016 Nov;17(6):32-43.
20. Nankali S, Torshabi AE, Miandoab PS. A feasibility study on ribs as anatomical landmarks for motion tracking of lung and liver tumors at external beam radiotherapy. Technology in cancer research & treatment. 2017 Feb;16(1):99-111.
21. Qiao H, Bai J. Dynamic simulation of FDG-PET image based on VHP datasets. InThe 2011 IEEE/ICME International Conference on Complex Medical Engineering. 2011 May 22 (pp. 154-158). IEEE.
22. Dimitrakopoulou-Strauss A, Georgoulias V, Eisenhut M, Herth F, Koukouraki S, Mäcke HR, Haberkorn U, et al. Quantitative assessment of SSTR2 expression in patients with non-small cell lung cancer using 68 Ga-DOTATOC PET and comparison with 18 F-FDG PET. European journal of nuclear medicine and molecular imaging. 2006 Jul;33:823-30.
23. Wienhard K. Measurement of glucose consumption using [18F] fluorodeoxyglucose. Methods. 2002 Jul 1;27(3):218-25.
24. Sokoloff L, Reivich M, Kennedy C, Rosiers MD, Patlak CS, Pettigrew KE, et al. The [14C] deoxyglucose method for the measurement of local cerebral glucose utilization: theory, procedure, and normal values in the conscious and anesthetized albino rat 1. Journal of neurochemistry. 1977 May;28(5):897-916.
25. Feng D, Huang SC, Wang X. Models for computer simulation studies of input functions for tracer kinetic modeling with positron emission tomography. International journal of bio-medical computing. 1993 Mar 1;32(2):95-110.
26. Feng D, Wang X. A computer simulation study on the effects of input function measurement noise in tracer kinetic modeling with positron emission tomography (PET). Computers in biology and medicine. 1993 Jan 1;23(1):57-68.
27. Feng D, Li X, Huang SC. A new double modeling approach for dynamic cardiac PET studies using noise and spillover contaminated LV measurements. IEEE transactions on biomedical engineering. 1996 Mar;43(3):319-27.
28. Feng D, Wang X. A method for biomedical system modelling and physiological parameter estimation using indirectly measured input functions. International journal of systems science. 1995 Apr 1;26(4):723-39.
29. Thielemans K, Tsoumpas C, Mustafovic S, Beisel T, Aguiar P, Dikaios N, Jacobson MW. STIR: software for tomographic image reconstruction release 2. Physics in Medicine & Biology. 2012 Jan 31;57(4):867.
30. Loening AM, Gambhir SS. AMIDE: a free software tool for multimodality medical image analysis. Molecular imaging. 2003 Jul 1;2(3):15353500200303133.